Determination of Active-site Conformations in Paramagnetic Myoglobin from Analyses of Cross-relaxation and Hyperfine Shifts

Yasuhiko Yamamoto
Department of Chemistry, University of Tsukuba, Tsukuba 305, Japan

A methodology for determining the haem vinyl, haem propionate α-CH_2 and proximal His F8 C_α–C_β conformations in the active site of haemoproteins has been elaborated. It is based on measurements of interproton distances using the time-dependent nuclear Overhauser effect (NOE) and analysis of hyperfine shifts. The initial build-up slope of the NOE between selected protons for each fragment provides the cross-relaxation rate which can be interpreted in terms of the interproton distance. Secondary NOEs and spin diffusion are observed for the met-cyano form of myoglobin used. However, the primary NOE can be identified from the initial NOE build-up slope. Owing to the symmetric nature of the fragments, two conformational states are obtained for a given interproton distance. The analysis of the hyperfine shifts provides complementary structural information to that obtained from the NOE results. Consequently, specific conformations for these fragments can be uniquely determined from combined analyses of the cross-relaxation rates and hyperfine shifts.

The functional properties of haemoprotein crucially depend on the haem molecular/electronic structure[1] (Fig. 1). Interaction between the π system of the peripheral vinyl group and the π-conjugated system of the haem is thought to influence the electronic structure of the latter.[3,4] The conformations of the propionate groups have shown to be important for haem–protein interaction.[5–10] The orientations of these peripheral side-chains with respect to the haem were defined using crystallographic techniques.[11,12] Since NMR spectroscopy can be used to study such local conformations in the active site of haemoprotein in solution, it is of importance to compare the conformations of the haem side-chains determined by NMR spectroscopy with those obtained crystallographically. Two NMR methodologies have been proposed for this purpose: two-dimensional nuclear Overhauser effect correlated spectroscopy (NOESY) which is applicable to both paramagnetic and diamagnetic haemoproteins;[13] and multidimensional NMR spectroscopy for diamagnetic haemoproteins.[14] The former method is based on the determination of interproton distances using the cross-relaxation rates obtained from the time evolution of NOESY cross-peaks. However, the analysis of interproton distances leads to two possible conformations. In the latter method it was shown that the conformations can be uniquely determined from the analyses of NOESY cross-peaks and spin–spin coupling constants. For large haemoproteins, however, increased linewidths render the measurements of spin–spin coupling constants unrealistic.

In the present study the conformations of three typical fragments in the active site of b-type haemoprotein, *i.e.*, haem vinyl, haem propionate α-CH_2 and proximal His F8 C_α–C_β conformations, are considered (see Fig. 2). As shown, the conformation of each fragment is defined by a single dihedral angle. In Fig. 3 the distances between selected protons for each fragment are plotted as a function of the dihedral angles defined in Fig. 2. It is obvious in Fig. 3 that, owing to the symmetric nature of the fragment, two conformational states are obtained with a given interproton distance. Hence, additional structural information is needed for specific determination of their conformations. In the NMR analyses of paramagnetic haemoproteins the paramagnetic relaxation and hyperfine shift provide sensitive probes for molecular structure of the haem active site.[13,15–21] Although paramagnetic relaxation is useful to assess the distance from the paramagnetic centre (R_{Fe-H})

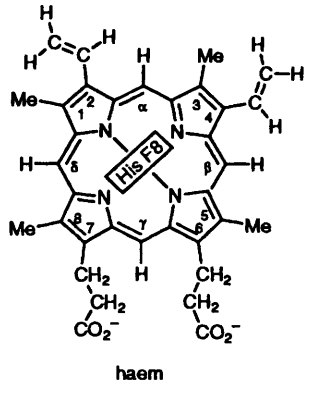

Fig. 1 Structure and numbering system of haem. The rectangle represents the plane of the proximal His F8 imidazole as found in the crystal structure of sperm whale myoglobin[2]

through the inverse 6th-power dependency of the relaxation rate on R_{Fe-H},[22] R_{Fe-H} is relatively insensitive to the conformational changes of the fragments considered in the present study. On the other hand, hyperfine shifts are particularly sensitive to the conformations of the haem peripheral side-chains, because both contact and pseudo-contact shifts for the resonances arising from protons attached to these side-chains are largely modulated by the dihedral angles defined in Fig. 2(*a*) and 2(*b*). Similarly to the case based on the analysis of interproton distances, the analysis of hyperfine shifts could also provide two possible conformations for each fragment. However, combined analyses of both interproton distances and hyperfine shifts could lead to the specific determination of their conformations.

Herein the results of a conformational study on haem vinyl, haem propionate α-CH_2 and proximal His F8 C_α–C_β fragments in the active site of the met-cyano complex of shark (*Galeorhinus japonicus*) myoglobin are reported using combined analyses of both cross-relaxation rates and hyperfine shifts. Secondary NOEs and spin diffusion are observed for the present sample. However, detailed time-dependent NOE measurements allowed differentiation of primary NOEs from others. Time-dependent NOE analysis provides two possible

conformations for a given fragment and the analysis of hyperfine shifts independently leads to complementary structural information to that from the NOE analysis. The determined conformations of these side-chains in the shark myoglobin were compared with those in the crystal structure of sperm whale myoglobin.[2]

Materials and Methods

Sample Preparation.—Myglobin was extracted from red muscle of the shark (*Galeorhinus japonicus*) and purified using the reported procedure.[23,24] It was then oxidized by addition of a five-fold molar excess of $K_3[Fe(CN)_6]$ to prepare the iron(III) form of myoglobin and passed through a Sephadex G-50 (Sigma Chemical Co.) column equilibrated with 10 mmol dm^{-3} Bis-Tris buffer $\{N(CH_2CH_2OH)_2[C(CH_2OH)_2CH_2OH]\}$ pH 6.80. A 10-fold molar excess of potassium cyanide was added to the iron(III) myoglobin to prepare met-cyanomyoglobin. This was concentrated to about 0.5 mmol dm^{-3} in an Amicon ultrafiltration cell and the solvent was exchanged to ^2H_2O. The pH value of the sample was measured using a Horiba F-22 pH meter equipped with a Horriba 6069-10C electrode. It was not corrected for isotope effects.

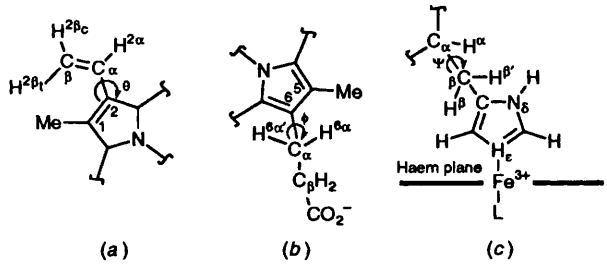

Fig. 2 (*a*) Dihedral angle θ is defined as the angle between the 2-vinyl plane and the normal to the haem plane; θ = 0° for the vinyl plane orthogonal to the haem plane with $H^{2\beta t}$ oriented in the proximal His F8 side with respect to the haem plane and +90° for C_α–C_β *cis* to C^2–C^1. (*b*) Dihedral angle φ is defined as the angle between the plane comprising of C^6, C_α, C_β and the normal to the haem plane; φ = 0° for the C^6, C_α, C_β plane orthogonal to the haem plane and +90° for C_α–C_β *cis* to C^6–C^5. Owing to the symmetric nature of the $C_6C_\alpha H_2$ fragment, the angles φ and φ + 180° (or φ − 180°) cannot be differentiated. (*c*) Dihedral angle ψ is defined by the atoms $HC_\alpha C_\beta H$ of the proximal His F8 side-chain; ψ = 0° for $C_\alpha H$ eclipsed by $C_\beta H$. The C_β methylene proton located closest to haem iron is labelled β and the other β′; NMR differentiation of these two protons in paramagnetic haemoprotein can easily be carried out from the comparison of their relaxation times or hyperfine shifts. The rotation direction for ψ is positive when the viewer is located on the C_α atom and observes a clockwise rotation around the C_α–C_β bond

NMR Measurements.—Proton NMR spectra were recorded on a Bruker AC-400P FT spectrometer operating at 400 MHz. A typical spectrum was recorded with 2000 transients, spectral width 25 kHz, 8k data points and 10.5 μs 90° pulse. The residual water resonance was suppressed with a 350 ms presaturation decoupler pulse. The NOE difference spectra were recorded by selectively saturating a desired peak for a variety of times and the results are presented in the form of NOE difference spectra. Chemical shifts are given in ppm downfield from sodium 4,4-dimethyl-4-silapentanesulfonate with the residual H^2HO as internal reference.

Interproton distance determination from cross-relaxation. Time-dependent NOE was used to determine the interproton distance. The time evolution of an NOE observed for a peak of spin *i* upon saturating a peak of spin *j* in a two-spin system can be represented by[25] equation (1) where σ_{ij} is the rate of the

$$NOE_i(t) = (\sigma_{ij}/\rho_i)[1 - \exp(-\rho_i t)] \quad (1)$$

cross-relaxation between the spins and ρ_i is the rate of the intrinsic spin–lattice relaxation for spin *i*. For a short saturation time *t* for spin *j*, the truncated NOE is given by equation (2).

$$NOE_i(t) = \sigma_{ij} t \quad (2)$$

Consequently the NOE build-up rate is independent of ρ_i and is simply proportional to σ_{ij};[26] σ_{ij} is related to the mobility of the interproton vector between the interacting spins.[22] Provided that two interproton vectors undergo identical motion, the ratio of the σ values, σ_1 and σ_2, for two systems is simply expressed as the ratio of the interproton distances, R_2 and R_1, as in equation (3).

$$\sigma_1/\sigma_2 = (R_2/R_1)^6 \quad (3)$$

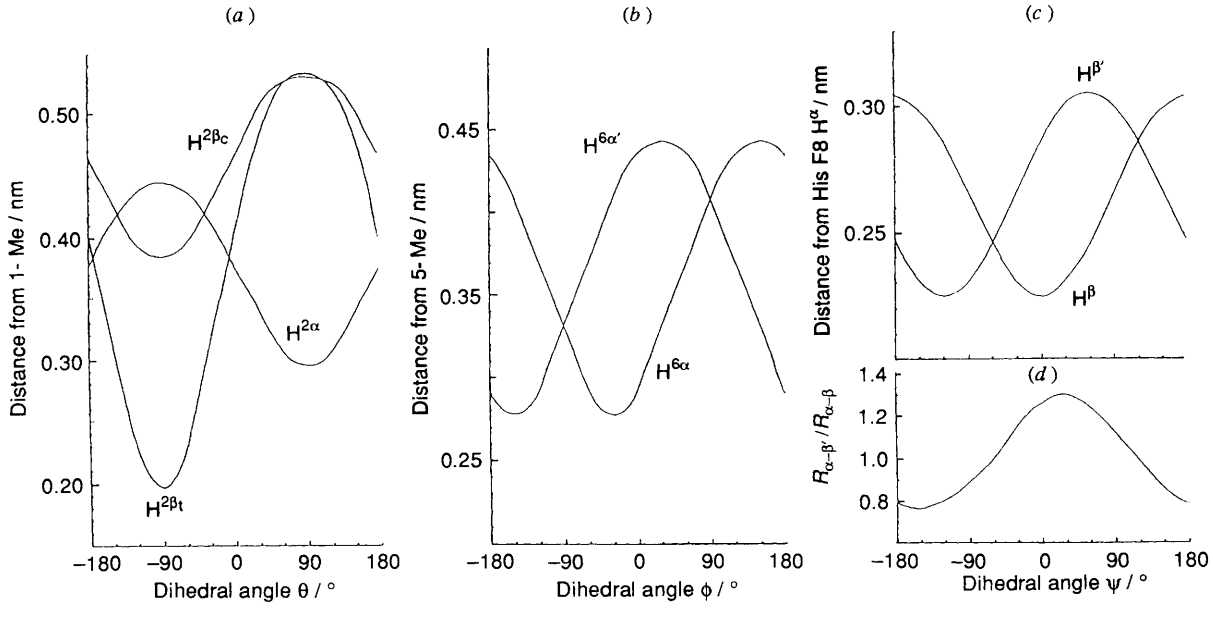

Fig. 3 (*a*) Plot of θ *versus* the distances of the 2-vinyl protons from the 1-Me proton. (*b*) Plot of φ *versus* the distances of the 6-propionate H^α protons from the 5-Me proton. (*c*) Plot of ψ *versus* the distances of the proximal His F8 H^β and $H^{\beta'}$ protons from H^α. (*d*) Plot of ψ *versus* the ratio of the $(H^\alpha \cdots H^{\beta'})$ and $(H^\alpha \cdots H^\beta)$ distances, $R_{\alpha-\beta'}/R_{\alpha-\beta}$

Since the time-scale for haem methyl rotation is at least three orders of magnitude smaller than that for haem vinyl and propionate mobility,[27-30] the centre of mass for the methyl protons is used to calculate distances. For the analysis of the proximal His F8 C_α–C_β conformation, the angle ψ defined in Fig. 2(*c*) is assumed to be independent of time.

Results and discussion

Determination of the Haem Vinyl Conformation.—The 400 MHz ^{1}H NMR spectrum of the shark met-cyanomyoglobin in ^2H_2O, pH 8.51, at 45 °C is illustrated in Fig. 4. Several haem peripheral side-chain proton resonances and proximal His F8 proton resonances are paramagnetically shifted and clearly resolved from the diamagnetic envelope, δ 0–10, where signals for the protein overlap severely. These resonances have been assigned using two-dimensional NMR spectroscopy.[18,21]

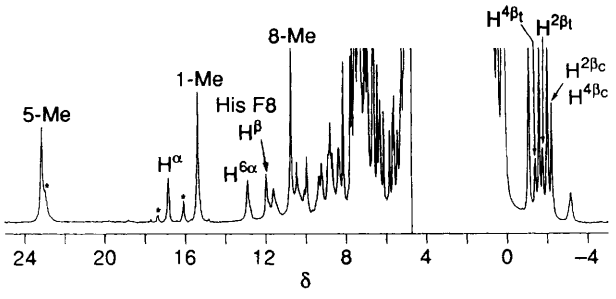

Fig. 4 The 400 MHz ^{1}H NMR spectrum of shark met-cyanomyoglobin in ^2H_2O, p^{2}H 8.51, at 45 °C. Signal assignments[18,21] are indicated. The $H^{2\beta c}$ and $H^{4\beta c}$ resonances degenerate at this temperature. There is another signal resonating under the His F8 H^β resonance. Peaks labelled * are not due to haem orientational disorder[31,32] and possibly arise from impurities

The NOE difference spectra upon saturation of the $H^{2\beta t}$ resonance for a variety of times are illustrated in Fig. 5(*a*). Saturation of the $H^{2\beta t}$ signal results in negative NOE to the 1-Me, $H^{2\alpha}$ and $H^{2\beta c}$ signals. The NOEs were calculated using the integration of signals in the NOE difference spectra. The time evolution of the NOEs is plotted against the saturation time of $H^{2\beta t}$ in the inset. The initial NOE build-up slope for the plot of $H^{2\alpha}$ vanishes at $t > 0$, indicating that the NOE for this proton is secondary. The initial slopes for 1-Me and $H^{2\beta c}$ provide the σ values of -0.090 ± 0.01 and -1.3 ± 0.1 s^{-1}, respectively. Since the 1-Me–$H^{2\beta t}$ and $H^{2\beta t}$–$H^{2\beta c}$ vectors are expected to undergo identical internal motion, the σ values obtained can be interpreted in terms of the interproton distances using equation (3). Thus, using the known $H^{2\beta c}$–$H^{2\beta t}$ distance (0.177 nm), a value of 0.28 ± 0.1 nm is obtained for 1-Me–$H^{2\beta t}$. This distance corresponds to the θ values of about −40 and about −140° in Fig. 3(*a*). With these conformations, $H^{2\beta t}$ is closer to 1-Me than are $H^{2\alpha}$ and $H^{2\beta c}$. The order of distances 1-Me–$H^{2\beta t}$ < 1-Me–$H^{2\alpha}$ and 1-Me–$H^{2\beta c}$ is clearly reflected in the NOE difference spectra shown in Fig. 5(*b*). Upon saturation of the 1-Me proton resonance, a faster NOE build-up for $H^{2\beta t}$ than for $H^{2\beta c}$ confirms that the former proton is closer to 1-Me. Significant effects of spin diffusion can be seen on peaks in the diamagnetic region of the spectra.

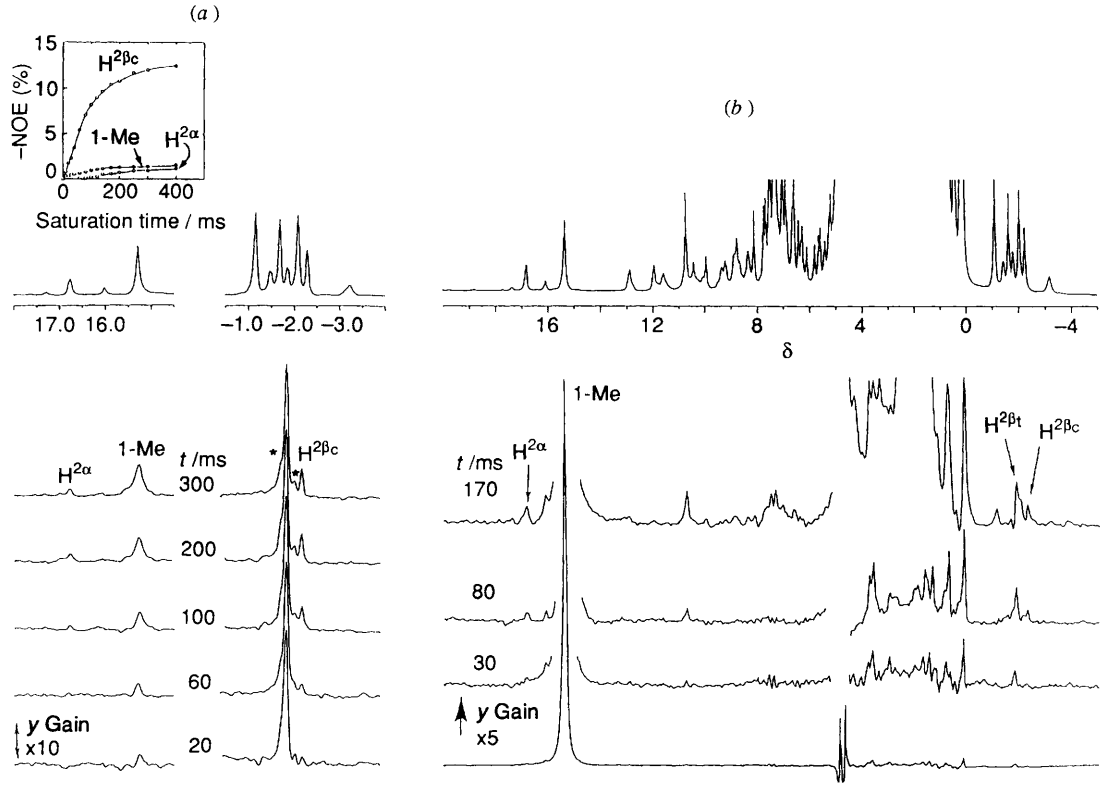

Fig. 5 Time-dependent NOE. (*a*) Observed upon saturation of the $H^{2\beta t}$ signal for the indicated time at 45 °C. The *y* scale for the $H^{2\alpha}$ and 1-Me signals is expanded by a factor of 10 and these signals are apodized with a larger line-broadening factor to improve the signal-to-noise ratio. Peaks labelled * are due to decoupler pulse-power spillage. The time evolution of the NOEs observed for the 1-Me, $H^{2\alpha}$ and $H^{2\beta c}$ signals upon saturating $H^{2\beta t}$ is indicated in the inset. That for $H^{2\alpha}$ clearly indicates that the NOE for this proton is secondary. The initial build-up slopes of the other two protons provide the σ values -0.090 ± 0.01 and -1.3 ± 0.1 s^{-1} for 1-Me and $H^{2\beta c}$, respectively. (*b*) Observed upon saturation of the 1-Me signal for the indicated time at 45 °C. The *y* gain of the spectra in the inset is expanded by a factor of 5 relative to that of the spectrum of the bottom and the intensity of the 1-Me proton resonance is kept constant. The NOE build-up rate for $H^{2\beta t}$ is larger than that for $H^{2\beta c}$, clearly indicating that the former proton is closer to the 1-Me. The peaks in the diamagnetic region result from the spin diffusion. Build-up of $H^{2\alpha}$ would be attributed to secondary NOE and decoupler pulse-power spillage; NOE to 8-Me is also clearly observed

Analysis of the hyperfine shifts for the $H^{2\beta c}$ and $H^{2\beta t}$ resonances provides another estimate for θ. The orientation of the principal magnetic axes with respect to haem in shark metcyanomyoglobin in solution was reported previously.[18] With the principal magnetic axes, the metal-centred dipolar field can be quantitated and hence the pseudo-contact shift for a given nucleus can be calculated from its coordinates with respect to the principal axes. The difference in the calculated pseudo-contact shift between the $H^{2\beta c}$ and $H^{2\beta t}$ resonances is plotted against θ in Fig. 6. At 35 °C the difference in the hyperfine shift between these resonances is −0.13 ppm [$\delta(H^{2\beta t}) - \delta(H^{2\beta c})$]. Assuming that this difference arises solely from the pseudo-contact-shift contribution, this value corresponds to the θ values of −36 and +10° in Fig. 6. Consequently, a θ value of about −40° satisfies the results from both NOE and hyperfine-shift analyses and these results give strong support to the contact-shift contributions for $H^{2\beta c}$ and $H^{2\beta t}$ being similar. Thus the haem 2-vinyl group in the myoglobin complex appears to point toward the proximal side with θ about −40°.

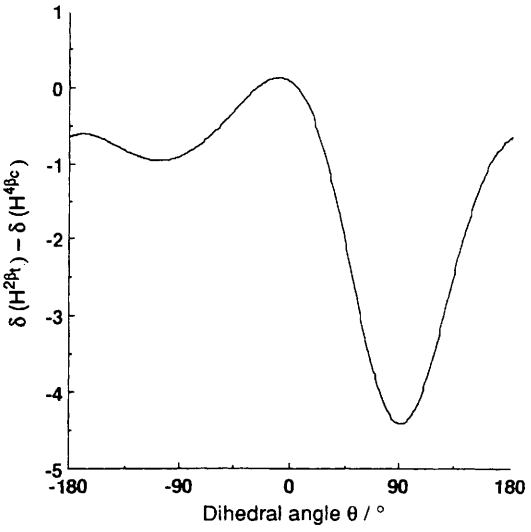

Fig. 6 Plot of θ *versus* the difference in the pseudo-contact shift, $\delta(H^{2\beta t}) - \delta(H^{2\beta c})$[18]

Determination of the Haem Propionate α-CH_2 Conformation.—The NOE difference spectra upon saturation of the haem propionate $H^{6\alpha}$ signal at δ 12.9 for a variety of times at 45 °C are illustrated in Fig. 7(*a*). Saturation of $H^{6\alpha}$ results in NOEs to 5-Me and the other haem propionate α-CH proton, $H^{6\alpha'}$, at δ 7.4. Analysis of the pseudo-contact shifts for $H^{6\alpha}$ and $H^{6\alpha'}$ signals based on the orientation of the principal magnetic axes[18] indicated that the difference in their pseudo-contact shifts should be $< \approx 2$ ppm for a given φ value. Furthermore, since pseudo-contact and contact shift contributions shift these resonances up- and down-field, respectively, it is concluded that the contact shift for $H^{6\alpha}$ is larger than that for $H^{6\alpha'}$. The NOE

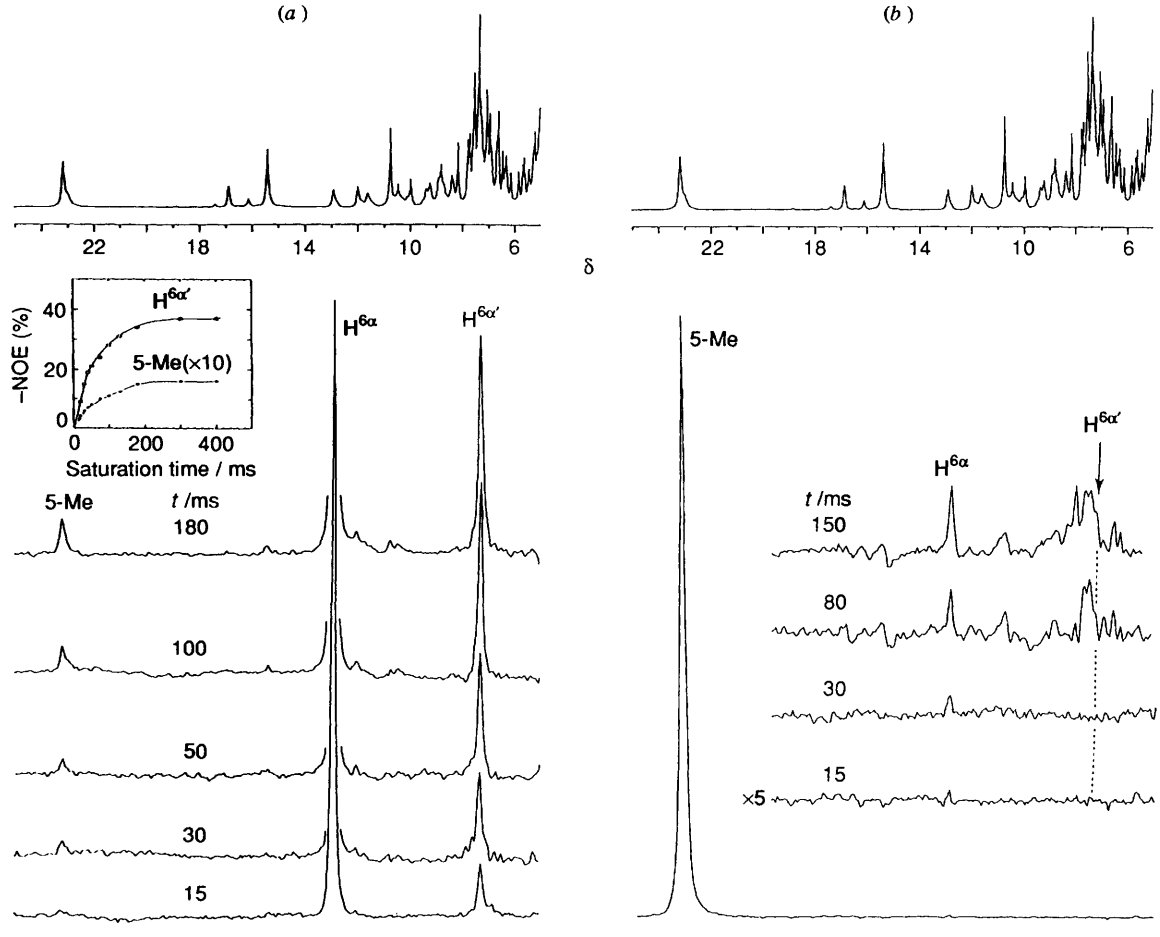

Fig. 7 Time-dependent NOE. (*a*) Observed upon saturation of the $H^{6\alpha}$ signal for the indicated time at 45 °C. In the difference spectra the intensity of this resonance is kept constant. The time evolution of the NOE observed on $H^{6\alpha'}$ and 5-Me is in the inset; that for 5-Me is multiplied by 10. The initial build-up slopes provided σ values of −0.47 ± 0.01 and −0.020 ± 0.005 s^{-1} for $H^{6\alpha'}$ and 5-Me, respectively. (*b*) Observed upon saturating the 5-Me signal for the indicated time at 45 °C. The *y* scale of the difference spectra in the inset are expanded by a factor of 5 relative to that of the spectrum at the bottom and the intensity of the 5-Me proton resonance is kept constant. The fact that the NOE build-up rate for $H^{6\alpha}$ is larger than that for $H^{6\alpha'}$ indicates that the former is closer to 5-Me

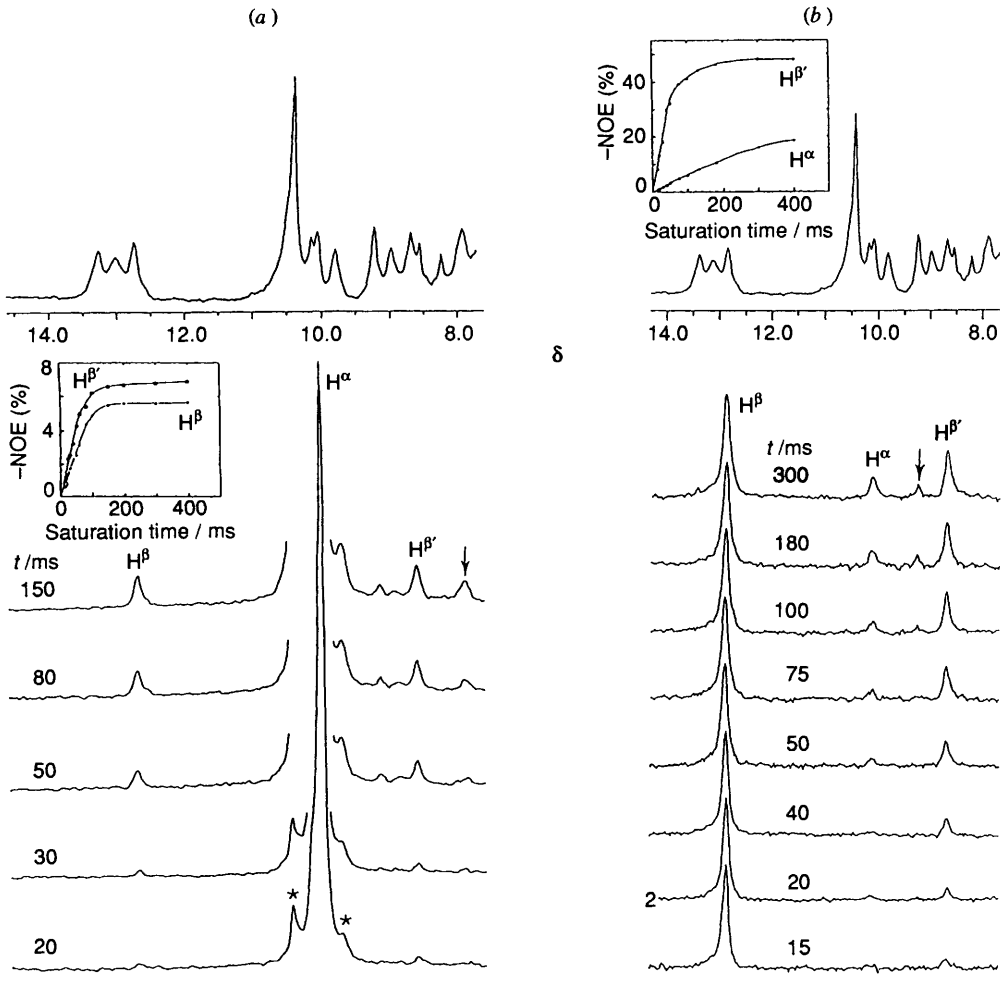

Fig. 8 Time-dependent NOE. (*a*) Observed upon saturation of the proximal His F8 H^{α} signal for the indicated time at 30 °C. The intensity of H^{α} is kept constant. The time evolution of the NOE observed for the His F8 H^{β} and $H^{\beta'}$ protons is illustrated in the inset and the initial build-up slopes provide σ values of -0.58 ± 0.01 and -0.81 ± 0.01 s^{-1} for H^{β} and $H^{\beta'}$, respectively. Comparison of these σ values yields 0.95 ± 0.01 : 1 for the ratio of the (H^{α}–$H^{\beta'}$) and (H^{α}–H^{β}) distances, $R_{\alpha-\beta'}/R_{\alpha-\beta}$. (*b*) Observed upon saturation of the proximal His F8 H^{β} signal for the indicated time at 30 °C. The time evolution of the NOE observed for the His F8 H^{α} and $H^{\beta'}$ are indicated in the inset. The initial build-up slopes provided σ values of -0.63 ± 0.03 and -6.8 ± 0.1 s^{-1} for H^{α} and $H^{\beta'}$, respectively. Peaks indicated by an arrow are due to secondary NOE

build-up curves for 5-Me and $H^{6\alpha'}$ are shown in the inset. The initial NOE build-up slopes provide σ values of -0.020 ± 0.005 and -0.47 ± 0.01 s^{-1} for 5-Me and $H^{6\alpha'}$, respectively from which, using the known distance for geminal protons, a distance of 0.30 ± 0.01 nm for 5-Me–$H^{6\alpha}$ is calculated. The former distance corresponds to φ values of about -70 and $+10°$ in Fig. 3(*b*). The saturation of 5-Me results in NOEs to both $H^{6\alpha}$ and $H^{6\alpha'}$ [see Fig. 7(*b*)] and the NOE build-up to $H^{6\alpha'}$ is quite slow. These results indicate that $H^{6\alpha}$ is closer to 5-Me than $H^{6\alpha'}$. The NOE build-up rate for $H^{6\alpha'}$ should be 33 and 10% of that for $H^{6\alpha}$ with the φ values of -70 and $+10°$ respectively obtained from the NOE analysis. The results in Fig. 7(*b*) support the value of $+10°$ for φ. Thus the plane consisting of C^{6}, C_{α} and C_{β} atoms in Fig. 2(*c*) appears to be close to orthogonal to the haem plane.

Contact shifts for the $H^{6\alpha}$ and $H^{6\alpha'}$ signals can be interpreted in terms of the φ value.[18,28] The larger contact shift for $H^{6\alpha}$ than for $H^{6\alpha'}$ indicates that the s orbital of $H^{6\alpha}$ interacts with the p_z orbital of C^{6} more than that of $H^{6\alpha'}$. Hence, the value of $+10°$ for φ obtained from the NOE analysis is completely consistent with the conformation predicted from the analysis of the hyperfine shifts for the $H^{6\alpha}$ and $H^{6\alpha'}$ signals. As long as the haem propionate α-CH_2 proton resonances exhibit a sizable shift difference, for example, $> \approx 2$ ppm, the φ value can be uniquely determined from the combined analyses of both interproton distances and hyperfine shifts.

Similar φ values for the haem 6-propionate group have been reported for other myoglobins and haemoglobins.[2,14,33-35] The orientation of the haem propionate groups with respect to the haem in haemoproteins appears to be determined and stabilized by hydrogen-bonding interaction between the propionate carboxyl oxygen and an amino acid side-chain. In the crystal structure of sperm whale myoglobin,[2,11,12] the side-chain of Arg CD3 is hydrogen bonded to the haem 6-propionate. In shark myoglobin, Arg CD3 is replaced by Lys CD3[36] and the ε-NH_3^+ of the Lys residue is likely to donate a proton to the haem 6-propionate to form a hydrogen bond. Thus, as has been pointed out,[14] a φ value close to 0° for the haem 6-propionate group in haemoproteins may be indicative of the presence of a hydrogen-bonding interaction between it and an amino acid residue at position CD3.

Determination of the Proximal His F8 C_{α}–C_{β} *Conformation.*—For the analysis of the proximal His F8 C_{α}–C_{β} conformation measurements were carried out at 30 °C due to the signal overlap as shown in Fig. 4. The NOE difference spectra upon saturation of the proximal His F8 H^{α} for a variety of times are shown in Fig. 8(*a*). The NOE build-up for His F8 H^{β} and $H^{\beta'}$ is plotted in the inset. The plots yield σ values of -0.58 ± 0.01 and -0.81 ± 0.02 s^{-1} for His F8 H^{β} and $H^{\beta'}$, respectively. Using equation (3), these values yield 0.95 ± 0.01 : 1 for the ratio of the H^{α}–$H^{\beta'}$ and H^{α}–H^{β} distances,

which corresponds to the ψ values of -75 ± 5 and $+130 \pm 5°$ in the plot of ψ *versus* $R_{\alpha-\beta'}/R_{\alpha-\beta}$ in Fig. 3(*d*).

The NOE difference spectra upon saturation of the proximal His F8 H^{β} signal for a variety of times are illustrated in Fig. 8(*b*). The NOE build-up curves for His F8 H^{α} and $H^{\beta'}$ are shown in the inset. The initial build-up slopes provide σ values of -0.63 ± 0.03 and -6.8 ± 0.1 s^{-1} for H^{α} and $H^{\beta'}$, respectively. These provide a value of 0.26 ± 0.1 nm for the H^{α}–H^{β} distance, which corresponds to a ψ value of about $\pm 80°$ in Fig. 3(*c*). Consequently, the value $\psi \approx -80°$ satisfies the results from the analyses of the two sets of time-dependent NOE data in Figs. 8(*a*) and 8(*b*).

In the crystal structure of sperm whale myoglobin[2] the ψ value is about $+140°$. Hence, the present study indicates that there is a large difference in the His F8 side-chain conformation between shark and sperm whale myoglobins. The observed shifts for the His F8 H^{α}, H^{β} and $H^{\beta'}$ proton signals for shark met-cyanomyoglobin at 35 °C are 9.1, 12.6 and 8.5 ppm, respectively, and the corresponding values for sperm whale are 7.4, 11.2 and 6.2 ppm, respectively.[21] The significant differences in these shifts suggest the presence of considerable differences in the orientation of these three protons with respect to both haem and His F8 imidazole. Although haem methyl-proton hyperfine-shift patterns in the ^1H NMR spectra of met-cyano complexes of these two myoglobins suggest a possible difference in the orientation of the His F8 imidazole with respect to the haem,[37] the conformation of the His F8 side-chain defined by ψ in Fig. 2(*c*) is not directly correlated to the orientation of His F8 imidazole relative to the haem. A more detailed structural analysis is needed to interpret the observed large difference in ψ between the two myoglobins.

Conclusion

In spite of its lack of physiological significance, the met-cyano complex is useful for NMR determination of the active-site conformations in haemoprotein. Taking advantages of paramagnetism, the well resolved resonances and large peak separation provide an ideal system for measurements of NOE difference spectra. Although spin diffusion influences NOE measurements, detailed time-dependent NOE analyses enable us to differentiate between primary and secondary NOEs. Interproton distance information provides two possible conformations for each fragment considered in the present study. The analysis of hyperfine shifts independently yields structural information complementary to the NOE results. Consequently, the specific conformations of the haem vinyl, haem propionate α-CH_2 and proximal His F8 C_{α}–C_{β} fragments in myoglobin can be determined through combined analyses of cross-relaxation and hyperfine shifts. As has been demonstrated,[13] time-dependent NOE measurements can also be performed by a series of NOESY experiments using a variety of mixing times.

Acknowledgements

The author gratefully acknowledges Dr Tomohiko Suzuki (Kochi University) for the *Galeorhinus japonicus* myoglobin.

References

1 T. Asakura, P. W. Lau, M. Sono, K. Adachi, J. J. Smith and J. A. McCray, in *Hemoglobin and Oxygen Binding*, ed. C. Ho, Elsevier, New York, 1982, p. 177.
2 S. E. V. Phillips, *J. Mol. Biol.*, 1980, **142**, 531.
3 L. S. Reid, A. R. Lim and A. G. Mauk, *J. Am. Chem. Soc.*, 1986, **108**, 8197.
4 J. D. Satterlee and J. D. Erman, *J. Biol. Chem.*, 1983, **258**, 1050.
5 J. B. Hauksson, G. N. La Mar, R. K. Pandey, I. N. Rezzano and K. M. Smith, *J. Am. Chem. Soc.*, 1990, **112**, 6198.
6 J. B. Hauksson, G. N. La Mar, R. K. Pandey, I. N. Rezzano and K. M. Smith, *J. Am. Chem. Soc.*, 1990, **112**, 8315.
7 G. N. La Mar, J. B. Hauksson, L. B. Dugad, P. A. Liddel, N. Venkataramana and K. M. Smith, *J. Am. Chem. Soc.*, 1991, **113**, 1544.
8 G. N. La Mar, U. Pande, J. B. Hauksson, R. K. Pandey and K. M. Smith, *J. Am. Chem. Soc.*, 1989, **111**, 485.
9 S. Neya and N. Funasaki, *J. Biol. Chem.*, 1987, **262**, 6725.
10 S. Neya and N. Funasaki, *Biochim. Biophys. Acta*, 1988, **952**, 150.
11 J. Kuriyan, S. Wilz, M. Karplus and G. A. Petsko, *J. Mol. Biol.*, 1986, **192**, 133.
12 X. Cheng and B. P. Schoenborn, *J. Mol. Biol.*, 1991, **220**, 381.
13 M. Sette, J. S. de Ropp, G. Hernandez and G. N. La Mar, *J. Am. Chem. Soc.*, 1993, **115**, 5237.
14 D. Morikis, R. Brüschweiler and P. E. Wright, *J. Am. Chem. Soc.*, 1993, **115**, 6238.
15 J. D. Satterlee, *Annu. Rep. N.M.R. Spectrosc.*, 1986, **17**, 79.
16 J. D. Satterlee, *Met. Ions Biol. Syst.*, 1986, **21**, 121.
17 G. N. La Mar and J. S. de Ropp, *Biol. Magn. Reson.*, 1993, **12**, 1.
18 Y. Yamamoto, K. Iwafune, N. Nanai, R. Chujo, Y. Inoue and T. Suzuki, *Biochim. Biophys. Acta*, 1992, **1120**, 173.
19 Y. Yamamoto and T. Suzuki, *Biochim. Biophys. Acta*, 1993, **1163**, 287.
20 Y. Yamamoto, K. Iwafune, R. Chujo, Y. Inoue, K. Imai and T. Suzuki, *J. Mol. Biol.*, 1992, **228**, 343.
21 Y. Yamamoto, K. Iwafune, N. Nanai, A. Osawa, R. Chujo and T. Suzuki, *Eur. J. Biochem.*, 1991, **198**, 299.
22 I. Solomon, *Phys. Rev.*, 1955, **99**, 559.
23 T. Suzuki and T. Kisamori, *Compr. Biochem. Physiol.*, 1984, **78B**, 163.
24 T. Suzuki, T. Suzuki and T. Yata, *Aust. J. Biol. Sci.*, 1985, **38**, 347.
25 J. H. Noggle and R. E. Schirmer, *The Nuclear Overhauser Effect, Chemical Applications*, Academic Press, New York, 1971.
26 L. B. Dugad, G. N. La Mar and S. W. Unger, *J. Am. Chem. Soc.*, 1990, **112**, 1386.
27 S. Ramaprasad, R. D. Johnson and G. N. La Mar, *J. Am. Chem. Soc.*, 1984, **106**, 3632.
28 Y. Yamamoto, Y. Inoue, R. Chujo and T. Suzuki, *Eur. J. Biochem.*, 1990, **189**, 567.
29 Y. Yamamoto, R. Chujo and T. Suzuki, *Eur. J. Biochem.*, 1991, **198**, 285.
30 Y. Yamamoto, *J. Magn. Reson.*, 1994, **B103**, 72.
31 G. N. La Mar, D. L. Budd, D. B. Viscio, K. M. Smith and K. C. Langry, *Proc. Natl. Acad. Sci. USA*, 1978, **75**, 5755.
32 Y. Yamamoto, A. Osawa, Y. Inoue, R. Chujo and T. Suzuki, *Eur. J. Biochem.*, 1990, **192**, 225.
33 B. C. Barden, G. Arents, E. A. Padlan and W. E. Love, *J. Mol. Biol.*, 1994, **238**, 42.
34 W. Steigemann and E. Weber, *J. Mol. Biol.*, 1979, **129**, 309.
35 G. Fermi, M. Perutz, B. Shaanan and R. Fourme, *J. Mol. Biol.*, 1984, **175**, 159.
36 T. Suzuki, *Biochim. Biophys. Acta*, 1987, **914**, 170.
37 Y. Yamamoto, N. Nanai, R. Chujo and T. Suzuki, *FEBS Lett.*, 1990, **264**, 113.

Received 13*th May* 1995; *Paper* 5/01572C